Int J. Heat Mass Transfer Vol. 12, pp 1157–1169. Pergamon Press 1969. Printed in Great Britain

# CONDENSATION IN THE PRESENCE OF A NONCONDENSABLE GAS IN DIRECT CONTACT

YEHUDA TAITEL
Department of Mechanical Engineering, University of California, Berkeley, California

and

ABRAHAM TAMIR
Department of Chemical Engineering, University of California, Berkeley, California

(*Received* 29 *July* 1968 *and in revised form* 11 *November* 1968)

**Abstract**—This work analyses the effect of impurities of a noncondensable gas present in the bulk of a vapor in direct contact condensation. The physical model is a free laminar stream that is exposed to its own vapor atmosphere containing the inert gas. The solution is based on the boundary layer conservation equations and is obtained using an exact similarity solution and an approximate integral method.

The analysis predicts reduction in the heat transfer rates near the "leading edge" (small $x^*$), which may be significant depending on the concentration of the noncondensable gas and the temperature driving force. This effect is accentuated at lower pressures. Far downstream ($x^* > 1$) the reverse effect is observed, namely, the local heat flux becomes much higher compared to the case without the presence of noncondensables.

## NOMENCLATURE

$B$, constant, equation (26);
$C_p$, heat capacity at constant pressure;
$D$, diffusion coefficient;
$f$, dimensionless stream function, equation (17);
$F^*$, dimensionless temperature gradient, equation (B.12);
$F^*_m$, the value of $F^*$ for $T^*_i = 1$;
$L$, stream thickness;
$M$, molecular weight;
$N$, dimensionless constant, equation (25);
$P$, total pressure;
$Pr'$, Prandtl number, $C'_p\mu'/k'$;
$P^*$, $Pr' \dfrac{\mu\rho'}{\mu'\rho}$;
$q$, local heat flux;
$q_m$, local heat flux for $T^*_i = 1$;
$s$, diffusion boundary-layer thickness, $s(x)$;
$s^*$, dimensionless diffusion boundary layer thickness, $s(x)/L$;
$Sc$, Schmidt number, $\mu/\rho D$;
$t$, thermal boundary layer thickness, $t(x)$;
$t^*$, dimensionless thermal boundary layer thickness in the liquid, $t(x)/L$;
$T$, local temperature;
$T^*$, dimensionless temperature $(T - T_0)/(T_\infty - T_0)$;
$T_\infty$, temperature corresponding to the total pressure of the pure vapor;
$u$, longitudinal velocity;
$u^*$, dimensionless longitudinal velocity, $u/u_0$;
$u_0$, stream velocity, constant;
$v$, normal velocity;
$v^*$, dimensionless normal velocity, $Lv/\alpha'$;
$w$, dimensionless mass fraction of the noncondensable gas, equation (7);
$w^*$, $w/w_\infty$;
$x$, longitudinal coordinate;
$x^*$, dimensionless longitudinal coordinate, $x\alpha'/L^2u_0$;
$y$, normal coordinate.
$y^*$, dimensionless normal coordinate, $y/L$;

Greek symbols

- $\alpha'$, thermal diffusivity of the liquid, $k'/\rho' C_p'$;
- $\delta$, hydrodynamic boundary-layer thickness, $\delta(x)$;
- $\delta^*$, dimensionless hydrodynamic boundary layer thickness, $\delta/L$;
- $\eta$, similarity variable, equation (16);
- $\lambda$, latent heat of vaporization;
- $\lambda^*$, $\lambda\rho/C_p'\rho'(T_\infty - T_0)$;
- $\mu$, absolute viscosity, for vapor gas mixture when used without subscript;
- $\xi$, $s/\delta$ or $s^*/\delta^*$;
- $\rho$, density, for vapor–gas mixture when used without subscript;
- $\psi$, dimensionless stream function, equation (17).

Subscripts and superscripts

- 0, inlet, at $x = 0$;
- $\infty$, in the bulk;
- $g$, noncondensable gas;
- $i$, at the interface;
- $m$, for pure vapor;
- $v$, condensing vapor;
- $'$, liquid, also differentiation with respect to $\eta$;
- $*$, dimensionless variable.

## INTRODUCTION

It is well known that the presence of a noncondensable gas in the bulk of a vapor appreciably effects the efficiency of heat transfer in condensation. Experimental results reported elsewhere [1], show that a reduction of almost fifty percent may occur compared to the case where the vapor is pure. This drastic reduction has been mainly attributed to a build-up of a noncondensable gas at the liquid–vapor interface. Hence, the saturation temperature at the interface drops and reduces the temperature difference for heat transfer. It has also been shown [2] that this effect is generally more significant than the effect of interfacial resistance and is more appreciable at lower pressures.

Sparrow [3] was the first to formulate a theory, based on conservation laws alone, to evaluate this effect. His study and others [3, 4] were concerned with vapor condensation on a solid surface. This work, however, deals with direct contact condensation, namely, where the vapor is condensed directly on a stream of cold liquid. The practical importance of this investigation lies, for example, in the area of water desalination where direct contact heat transfer is now under intensive development [5].

## PHYSICAL MODEL AND BASIC EQUATIONS

The physical model is a free laminar stream of liquid with constant thickness. It is exposed to its own saturated vapor atmosphere containing a noncondensable gas. Condensation occurs since its inlet temperature is lower than that of the vapor. The velocity of the stream is relatively high and approaches a slug-type flow. The transport processes are carried out in a vapor–gas boundary layer formed due to interfacial drag. A schematic diagram of the model described is shown in Fig. 1.

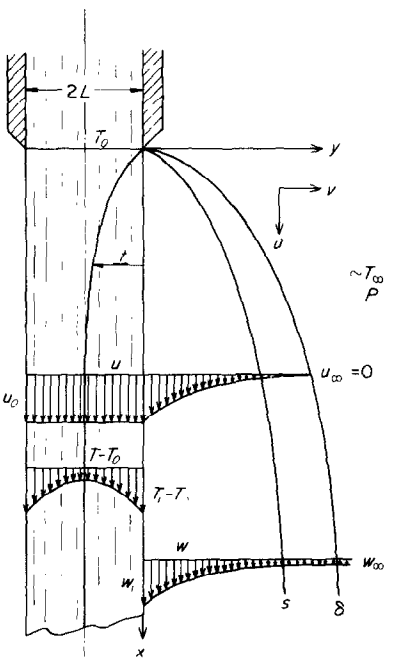


Fig. 1. Physical model and coordinate system.

The following assumptions were made:

(a) The thickness of the stream remains constant, neglecting the amount of vapor that condenses.
(b) The velocity everywhere in the stream is constant neglecting the interfacial drag.
(c) Free convection in the vapor–gas phase is negligible because of the relatively high velocities of the stream.
(d) The interface is impermeable to the noncondensable gas.
(e) Sensible heat effects are neglected; thus, energy equations in the vapor–gas phase are ignored [3].
(f) Interfacial resistance is negligible [2]. Thus, the vapor temperature at the interface is that of the liquid surface.
(g) In the liquid stream, axial conduction is assumed to be negligible compared to that in the transverse direction.
(h) Physical properties of the liquid and vapor–gas phases are constant.

The governing equations in a dimensionless form are given below:

*For the liquid stream*

$$\frac{\partial T^*}{\partial x^*} = \frac{\partial^2 T^*}{\partial y^{*2}}. \tag{1}$$

The boundary conditions are:

$$T^* = 0 \qquad \text{at} \quad x^* = 0 \tag{2}$$

$$\frac{\partial T^*}{\partial y^*} = 0 \qquad \text{at} \quad y^* = -1. \tag{3}$$

*For the vapor–gas boundary layer*

$$\frac{\partial u^*}{\partial x^*} + \frac{\partial v^*}{\partial y^*} = 0 \tag{4}$$

$$u^* \frac{\partial u^*}{\partial x^*} + v^* \frac{\partial u^*}{\partial y^*} = P^* \frac{\partial^2 u^*}{\partial y^{*2}} \tag{5}$$

$$u^* \frac{\partial w^*}{\partial x^*} + v^* \frac{\partial w^*}{\partial y^*} = \frac{P^*}{Sc} \frac{\partial^2 w^*}{\partial y^{*2}}. \tag{6}$$

The definition of the dimensionless (starred) values are given in the nomenclature. $w^* = w/w_\infty$ where $w$ is the local mass fraction of the noncondensable which is related to its partial pressure, assuming for this purpose ideal gas behavior, through the following equation:

$$w = \frac{\rho_g}{\rho} = \frac{1}{1 + \left(\frac{P}{P_g} - 1\right)\frac{M_v}{M_g}} = \frac{1}{1 + \left(\frac{P_v}{P - P_v}\right)\frac{M_v}{M_g}}. \tag{7}$$

The boundary conditions are:

$$u^* = 0, w^* = 1 \qquad \text{at} \quad x^* = 0 \tag{8}$$

$$-\frac{P^*}{Sc}\frac{\partial w^*}{\partial y^*} + w^* v^* = 0 \qquad \text{at} \quad y^* = 0 \tag{9}$$

where the last equation expresses assumption (d).

$$u^* = 0, \qquad w^* = 1 \qquad \text{at} \quad y^* \to \infty. \tag{10}$$

In addition we have the following matching boundary conditions at the interface:

$$u^* = 1, \qquad \frac{\partial T^*}{\partial y^*} = -v_i^* \lambda^* \qquad \text{at} \quad y^* = 0. \tag{11}$$

Also, as shown by equation (7), the noncondensable gas concentration at the interface is a function of the vapor partial pressure $P_{vi}$. Using an appropriate correlation relating vapor pressure to temperature for specific cases, one can get from equation (7) a relation between $T_i^*$ and $w_i$ or $w_i^*$, namely:

$$T_i^* = f\left(w_i^*, \frac{M_v}{M_g}, T_\infty, T_0, w_\infty\right) \tag{12}$$

Inspection of the above equations indicates that a particular solution depends on the parameters:

$$Sc, \lambda^*, P^*, \frac{M_v}{M_g}, \qquad P \text{ or } T_\infty, T_0, w_\infty \tag{13}$$

and the $P_v$–$T$ relation for the condensing vapor.

## SOLUTION

The problem was solved by two methods: an exact similarity solution which applies for small $x^*$ and an integral method which yields a solution for small and large $x^*$.

*Similarity solution*

Using a similarity transformation the equations of motion, continuity and diffusion (4), (5) and (6) yield a constant value for the interface temperature. Therefore the energy equation for the liquid stream (1) can be solved for $T_i^* =$ constant and the boundary conditions (2) and (3). The value of $T_i^*$ is later determined through the boundary condition (12) at the interface. Under these conditions the solution for the interfacial temperature gradient in the stream is found to yield [6]:

$$\frac{\partial T^*}{\partial y^*} = \frac{T_i^*}{\sqrt{(\pi x^*)}}\left[1 + 2\sum_{n=1}^{\infty}(-1)^n \exp\left(-n^2\frac{1}{x^*}\right)\right] \quad \text{at} \quad y^* = 0. \tag{14}$$

A similarity solution exists when the second term is negligible, namely, small $x^*$; hence:

$$\frac{\partial T^*}{\partial y^*} = \frac{T_i^*}{\sqrt{(\pi x^*)}} \quad \text{at} \quad y^* = 0. \tag{15}$$

In the vapor–gas phase the conservation equations (4) to (6) are solved by utilizing the following similarity variables:

$$\psi = \sqrt{(P^* x^*)} f(\eta) \quad \text{where} \quad \eta = y^* \sqrt{\left(\frac{1}{P^* x^*}\right)} \tag{16}$$

The velocity components are given by:

$$u^* = \frac{\partial \psi}{\partial y^*} = f'(\eta), \qquad v^* = -\frac{\partial \psi}{\partial x^*} = 0{\cdot}5\sqrt{\left(\frac{P^*}{x^*}\right)}[\eta f'(\eta) - f(\eta)]. \tag{17}$$

This leads to the following ordinary differential equations:

$$f'' f + 2f''' = 0 \tag{18}$$

$$w^{*\prime\prime} + 0{\cdot}5\, Sc\, f w^{*\prime} = 0 \tag{19}$$

where the differentiation is with respect to $\eta$. The transformed boundary conditions are:

$$\text{as} \quad \eta \to \infty: \quad f' = 0, w^* = 1 \qquad \text{at} \quad \eta = 0: \quad f' = 1, f = f_i \tag{20}$$

and

$$w^{*\prime} + 0{\cdot}5\, Sc\, f_i w^* = 0. \tag{21}$$

Use of the matching conditions (11) yields

$$f_i = \frac{2}{\sqrt{\pi}} \frac{T_i^*}{\lambda^* \sqrt{P^*}} = \text{constant}. \tag{22}$$

Equations (18) and (19) were solved for given values of $f_i$ which is determined later for a specific system by condition (12). For computational purposes, equations (18) and (19) were transformed into integral equations which are given in Appendix A. The momentum equation was solved by a an iterative procedure whereas the concentration distribution was directly obtained by numerical integration. The computations were performed on a CDC 6400 computer. Results of

$$w_i^* \text{ vs. } \frac{\sqrt{\pi}}{2} f_i = \frac{T_i^*}{\lambda^* \sqrt{P^*}} \equiv N$$

were plotted on Fig. 2 for various Schmidt numbers. Computation time is of the order of a few seconds.

*The integral method*

The method is detailed in Appendix B. Polynomials of the second order were assumed for the velocity and concentration profiles in the vapor–gas boundary layer, and for the temperature in the liquid stream. Consequently a set of six equations was obtained and solved simultaneously.

For small $x^*$ (where $T_i^*$ is constant), the analysis leads to a very simple and useful equation applicable for Schmidt numbers larger than 1.

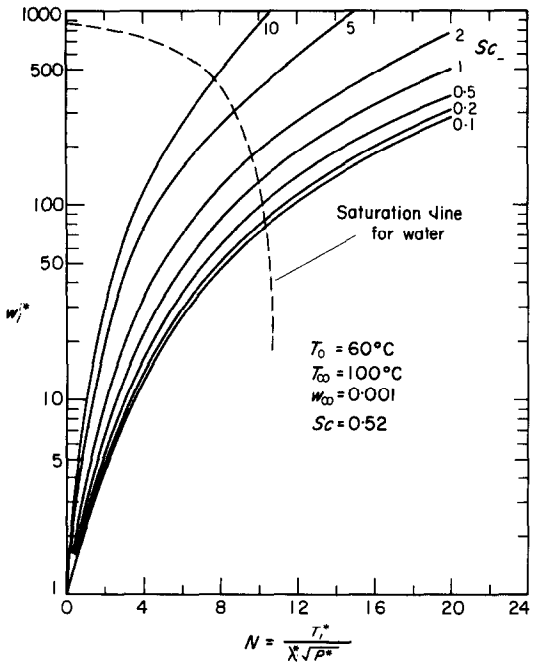


FIG. 2. Generalized curves of $w_i^*$ as a function of $N$ for small $x^*$.

$$w_i^* = (1 + 0{\cdot}5\,Sc\,N^2) + \sqrt{[(1 + 0{\cdot}5\,Sc\,N^2)^2 - 1]}. \quad (23)$$

For Schmidt numbers less than unity the following equation was obtained:

$$w_i^* = \frac{8(\sqrt{3})B + 24N - B^2 N\,Sc + \sqrt{\{[8(\sqrt{3})\,B + 24N - B^2 N\,Sc]^2 - 4[4(\sqrt{3})\,B - B^2 N\,Sc]\,[4(\sqrt{3})\,B + 24N]\}}}{8(\sqrt{3})\,B - 2B^2 N\,Sc} \quad (24)$$

where

$$N = \frac{T_i^*}{\lambda^* \sqrt{P^*}} \quad (25)$$

$$B = -\frac{5}{\sqrt{3}} N + \sqrt{\left(\frac{25}{3} N^2 + 20\right)}. \quad (26)$$

A comparison of the results obtained from equations (23) and (24) to those obtained from the similarity solution is summarized in Table 1. For Schmidt number equal to 2, for example, one can see that the results are almost identical, where in some other cases the error may reach 50 per cent. It was, however, found (see Figs. 3–7) that the maximum error introduced in $T_i^*$ for specific systems (water and carbon tetrachloride) is less than 15 per cent. Equations (23) and (24) therefore yield a valid approximation for the interface concentration of the noncondensable and its saturation temperature. The reason for the comparatively small error in $T_i^*$ is the steepness of the saturation line (see dashed line in Fig. 2). Thus the solution for $T_i^*$, obtained from the intersection of the $w_i^*$ curves [computed from equation (23) or (24)] with the saturation line, is not very sensitive to errors in $w_i^*$.

The solution for large $x^*$ ($\geqslant 1/12$) was obtained only for practical cases (Schmidt numbers less than unity) by numerical integration of the set of the ordinary differentiation equations (B 14–B.18). Typical results are given in Fig. 8.

## RESULTS AND DISCUSSION

The results for small $x^*$, obtained from the similarity solution, are summarized in Fig. 2 where the dimensionless interfacial concentration $w_i^*$ is plotted vs. $T_i^*/(\lambda^* \sqrt{P^*})$. The parameter in these curves is the Schmidt number which varies from 0·1 to 10. When applying these generalized curves for particular systems of liquid–vapor at given operating conditions, one needs in addition a relation between $w_i^*$ and $T_i^*$ (or $N$). This is obtained by substituting the correlation of vapor pressure–temperature into equation (7). Appendix C details these equations for water vapor and carbon tetrachloride. A typical example is given by the dashed line on Fig. 2. The intersection of this line with the solid line corresponding to a given Schmidt number defines $T_i^*$ and $w_i^*$. For practical purposes

*Table 1. Comparison of values of $w_i^*$ obtained from similarity solution and integral method*

| $Sc$ | 0·1 | | 0·2 | | 0·5 | | 1 | | | 2 | | 5 | | 10 | |
|---|---|---|---|---|---|---|---|---|---|---|---|---|---|---|---|
| $\frac{T_i^*}{\lambda^*\sqrt{P^*}}$ | *a* | *b* | *a* | *b* | *a* | *b* | *a* | *b* | *c* | *a* | *c* | *a* | *c* | *a* | *c* |
| 1 | 2·1 | 2·5 | 2·3 | 2·6 | 2·4 | 2·9 | 3·1 | 2·6 | 3·7 | 3·9 | 3·7 | 6·2 | 6·8 | 9·6 | 11·9 |
| 2 | 4·3 | 5·8 | 4·8 | 6·1 | 5·4 | 7·1 | 7·2 | 5·8 | 9·9 | 9·9 | 9·9 | 18·1 | 21·9 | 32·0 | 42·0 |
| 5 | 19·3 | 27·9 | 20·9 | 29·5 | 25·8 | 35·2 | 34·2 | 26·9 | 51·9 | 51·0 | 51·0 | 117·7 | 127·0 | 180·3 | 252·0 |
| 10 | 71·8 | 106·9 | 78·5 | 112·8 | 98·2 | 135·2 | 135·2 | 102·0 | 201·9 | 194·0 | 202·0 | 395·0 | 502·0 | 865·0 | 1002·0 |
| 15 | 159·4 | 238·5 | 174·4 | 251·7 | 218·7 | 301·9 | 289·3 | 227·0 | 452·0 | 433·4 | 452·0 | 990·0 | 1127·0 | — | — |

*a*—Results from exact solution (similarity solution).
*b*—Calculated by equation (24) for $\xi > 1$ (integral method).
*c*—Calculated by equation (23) for $\xi < 1$ (integral method).

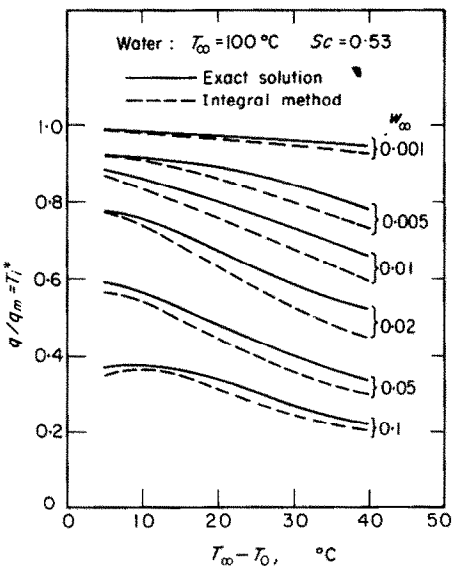


FIG. 3. Heat flux ratio for water at 760 mm Hg, small $x^*$.

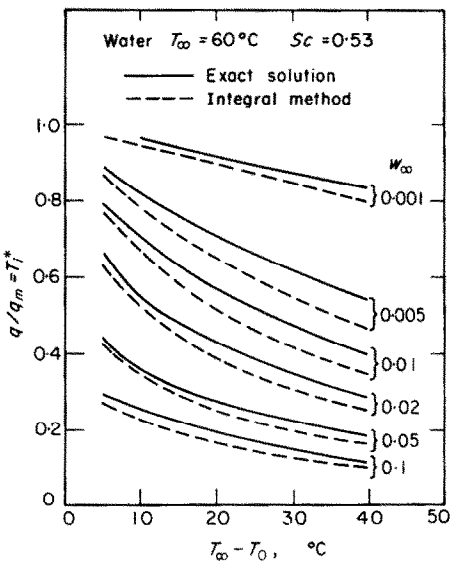


FIG. 4. Heat flux ratio for water at 150 mm Hg, small $x^*$

Appendix C includes also curves of $w_i$ vs. $T_i$ for several saturation temperatures ($T_\infty$). Use of these curves with Fig. 2 makes it possible to solve this problem conveniently by trial and error or graphically.

Numerical results for small $x^*$ are obtained for two systems. The first involves condensation of steam on a cooled water stream, while the other involves carbon tetrachloride condensing on its coolant, both in the presence of air as the noncondensable gas. The physical properties for these fluids were found or estimated from

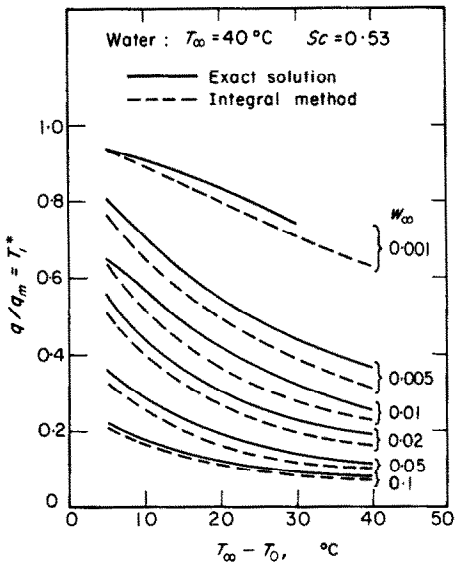


FIG. 5. Heat flux ratio for water at 55 mm Hg, small $x^*$.

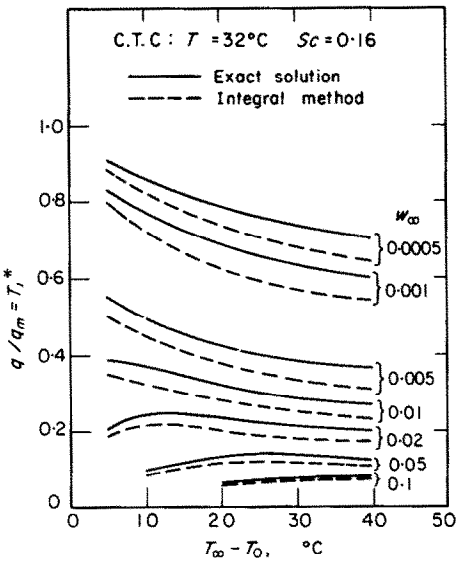


FIG. 7. Heat flux ratio for carbon tetrachloride at 150 mm Hg, small $x^*$.

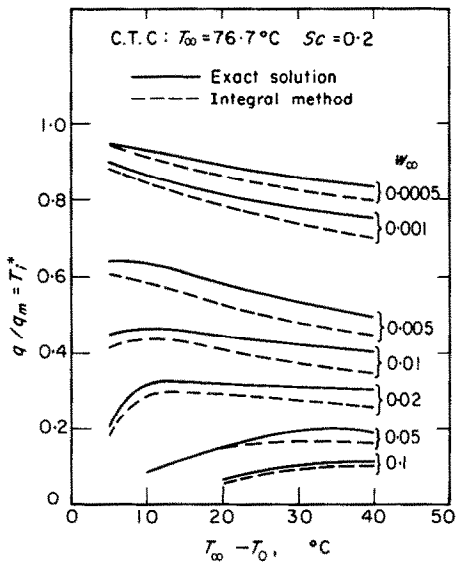


FIG. 6. Heat flux ratio for carbon tetrachloride at 760 mm Hg, small $x^*$.

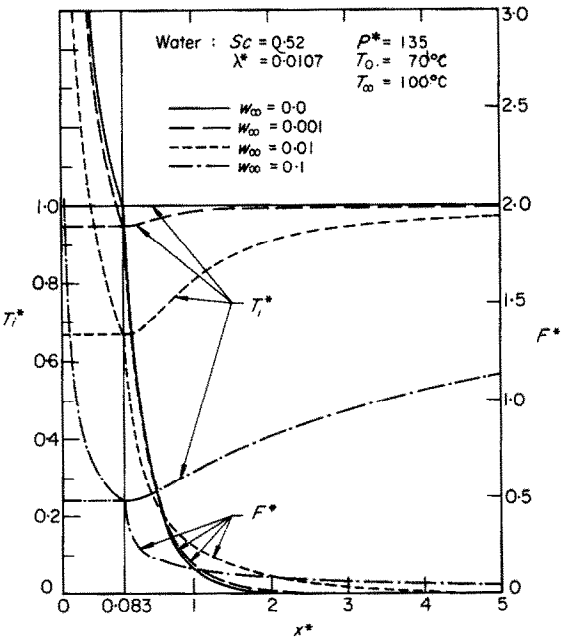


FIG. 8. Dimensionless interface temperature and temperature gradient along a water stream.

[7–9]. These results are shown in Figs. 3–7 where the heat transfer efficiency, $q/q_m$, is plotted vs. the thermal driving force, $T_\infty - T_0$, for various noncondensable concentration in the range of 0·0001 to 0·1 weight fraction and for several levels of pressure in the range of 50 mm Hg to atmospheric pressure. The ratio $q/q_m$ is obtained from equations (15) or (B.20) and is equal to $T_i^*$. The solid lines correspond to the exact solution while the broken lines are the result of the integral method. In general these graphs emphasize the effect of the noncondensables on reducing heat transfer efficiency, which is accentuated with increasing inert concentration, thermal driving force, and decreasing total pressure. It may also be observed that the system of carbon tetrachloride seems to be more sensitive than water to the presence of noncondensables under identical total pressure and $w_\infty$. However if molar fraction is used instead of weight fraction one finds that water and carbon tetrachloride behave roughly the same.

Results for the case where the condensation of steam occurs on a cooled solid surface were obtained by Mincowycz and Sparrow [2, 3]. Their report shows that the effect of inerts in reducing the heat flux is larger than in the case treated here which considers direct contact heat transfer. The general trends, however, are the same.

Experimental results have also been reported, primarily for condensation occurring on metallic surfaces. An investigation [10] which does consider direct contact condensation was recently reported for condensation of steam on water flowing in a tray. Comparison between the present analysis and the above mentioned work shows that the experimental values given there for the heat transfer coefficients are much higher than the ones predicted here. This is probably due to the fact that the flow over the plate was not laminar.

Solutions for the dimensionless interface temperature, $T_i^*$, and temperature gradient, $F^*$, for small and large $x^*$ were obtained using the integral method, for a typical system where saturated steam at 760 mm Hg is condensed on a water stream at an inlet temperature of 70°C. The results are contained in Fig. 8. The effect of the noncondensables is studied by considering a range of $w_\infty$ from 0 to 0·1. As would be expected, the value of the dimensionless interfacial temperature $T_i^*$ is unity for the ideal case of pure vapor. In the presence of air, the value of $T_i^*$ decreases when $w_\infty$ increases. This value is constant near the "leading edge" (the case where the similarity solution is valid) but increases as a function of $x^*$ to the asymptotic value $T_i^* = 1$ as $x^* \to \infty$. With respect to this we note that $T_i^*$ would be somewhat less than unity as $x^* \to \infty$ because of the small concentration of noncondensables in the bulk of the vapor.

Results for the dimensionless temperature gradient $F^*$ (proportional to the local heat flux) are also illustrated in Fig. 8. For the case where $w_\infty = 0$ a closed form solution is obtained

$$F^* = F_m^* = \frac{1}{\sqrt{(3x^*)}}; \qquad x^* \leqslant \frac{1}{12} \tag{27}$$

$$F^* = F_m^* = 2\exp(-3x^* + 0{\cdot}25); \qquad x^* \geqslant \tfrac{1}{12} \tag{28}$$

and is plotted by the solid line. In general the value for $F^*$ decreases for increasing $x^*$. It is interesting to observe that although for small $x^*$, (namely, near the "leading edge") the heat flux with noncondensables is less than without inerts ($F_m^* > F^*$), the reverse effect occurs for large $x^*$ where $F^* > F_m^*$. This phenomenon is explained as follows: In general the heat flux into the cold stream is governed by two factors—(a) the absolute value of $T_i^*$ and (b) its rate of increase along $x^*$. For a small rate of increase, it can be shown that near the "leading edge" the absolute value of the temperature difference is the dominant factor but it becomes negligible far downstream due to its exponential decay. Hence, in the downstream region the rate of increase of $T_i^*$ becomes the controlling factor. Although in our case the absolute value of $T_i^*$ is lower for higher concentrations of noncon-

densables, the heat flux for large $x^*$ is higher in these cases because of the higher rate of change of $T_i^*$ with $x^*$. This could also be seen by noting that the total heat delivered to the stream is approximately equal in all cases for large $x^*$ because the stream temperature reaches the equilibrium temperature of the bulk. Thus, the area under all curves of $F^*$ vs. $x^*$ should be almost equal. This, of course, means that if the value of $F^*$ is lower for small $x^*$ it must be higher for large $x^*$.

This characteristic behavior is completely different from the cases of condensation on solid surfaces, where it was found that the local conditions determine essentially the local heat flux due to the "poor memory" of the flow to upstream conditions [2]. This fact made it possible to use a local-similarity approximation for condensation on a plate. In the present case the upstream conditions are very important, and in fact are the dominant factors in the determination of the heat fluxes. It should be emphasized, however, that in spite of this interesting result the most important region is the one near the "leading edge", because in all cases this is the region of highest heat fluxes and most of the heat is transferred to the liquid through this region (unless the concentration of noncondensables is exceptionally large).

## CONCLUDING REMARKS

An analysis of the effect of noncondensables on direct contact condensation was carried out. An exact similarity solution for small $x^*$ and an integral solution for small and large $x^*$ are presented. The agreement between the two methods was tested for small $x^*$ and the integral method was found to predict heat transfer rates which deviate from the exact solution by less than 15 per cent (and which usually fall below the exact solution).

For small $x^*$, near the "leading edge", the interfacial temperature and heat fluxes decrease when the concentration of noncondensables is increased and when the total pressure is reduced. For large $x^*$ it was found that the local heat flux exceeds the flux for pure vapor.

## REFERENCES


1. D. F. Othmer, The condensation of steam, *Ind. Engng Chem.* **21**, 577–583 (1929).
2. W. J. Mincowycz and E. M. Sparrow, Condensation heat transfer in the presence of noncondensables, interfacial resistance, superheating, variable properties, and diffusion, *Int. J. Heat Mass Transfer* **9**, 1125–1144 (1966).
3. E. M. Sparrow and S. H. Lin, Condensation heat transfer in the presence of a noncondensable gas, *J. Heat Transfer* (C) **86**, 430–436 (1964).
4. E. M. Sparrow, W. J. Minkowycz and M. Saddy, Forced convection condensation in the presence of noncondensables and interfacial resistance, *Int. J. Heat Mass Transfer* **10**, 1829–1845 (1967).
5. A. Kogan, Heat and mass transfer in flash distillation without metalic interface, 1st Int. Symp. Water Desalin, Washington (1965) SWD/7.
6. H. S. Carslaw and J. C. Jaeger, *Conduction of Heat in Solids*, Oxford University Press, London (1959).
7. J. H. Perry, Chemical Engineers Handbook, 3rd Edn, McGraw-Hill, New York (1950).
8. *Handbook of Chemistry and Physics*, 37th Edn, Chemical Rubber Publishing Co., Cleveland, Ohio (1955).
9. R. B. Bird, W. E. Stewart and E. N. Lightfoot, *Transport Phenomena*, 3rd Edn, John Wiley, New York (1963).
10. S. E. Sadek, Condensation of steam in the presence of air. Experimental mass transfer coefficient in a direct-contact system, *I/EC Fundamentals* **7**, 321–324 (1968).
11. J. H. Keenan and F. G. Keyes, *Thermodynamics Properties of Steam*, John Wiley, New York (1955).


## APPENDIX A

### *The Integral Equations*

The integral form of equations (18) and (19) and the boundary conditions are:

$$f = f_i + \int_0^\eta f' \, d\eta \tag{A.1}$$

where

$$f' = 1 - \frac{\int_0^{\eta} \exp(-0{\cdot}5 \int_0^{\eta} f\, d\eta)\, d\eta}{\int_0^{\infty} \exp(-0{\cdot}5 \int_0^{\eta} f\, d\eta)\, d\eta} \tag{A.2}$$

$$w^* = 1 + \frac{0{\cdot}5\, Sc f_i (\int_0^{\infty} \exp(-0{\cdot}5 \int_0^{\eta} Sc f\, d\eta)\, d\eta - \int_0^{\eta} \exp(-0{\cdot}5 \int_0^{\eta} Sc f\, d\eta)\, d\eta)}{1 - 0{\cdot}5\, Sc f_i \int_0^{\infty} \exp(-0{\cdot}5 \int_0^{\eta} Sc f\, d\eta)\, d\eta}. \tag{A.3}$$

A solution for $f'$ is obtained by an iterative procedure using equations (A.1) and (A.2). The concentration profile is obtained by direct numerical integration of equation (A.3).

## APPENDIX B

### *The Integral Solution*

The momentum and diffusion equation (5) and (6), when integrated and combined with equation (4), yields the following integral equations:

$$\frac{\partial}{\partial x^*} \int_0^{\delta^*} u^{*2}\, dy^* - v_i^* = -P^* \left.\frac{\partial u^*}{\partial y^*}\right|_{y^*=0} \tag{B.1}$$

$$\frac{\partial}{\partial x^*} \int_0^{s^*} u^*(1 - w^*)\, dy^* = v_i^*.$$

Second-order polynomials were assumed for the velocity and concentration profiles:

$$u^* = 1 - 2\left(\frac{y^*}{\delta^*}\right) + \left(\frac{y^*}{\delta^*}\right)^2 \tag{B.2}$$

$$w^* = w_i^* - (w_i^* - 1)\left[2\left(\frac{y^*}{s^*}\right) - \left(\frac{y^*}{s^*}\right)^2\right]. \tag{B.3}$$

These profiles satisfy the following boundary conditions:

$$\text{at} \quad y^* = 0: \quad u^* = 1, \quad w^* = w_i^*(x^*) \tag{B.4}$$

$$\text{at} \quad y^* = \delta^*(x^*): \quad u^* = 0, \quad \partial u^*/\partial y^* = 0 \tag{B.5}$$

$$\text{at} \quad y^* = s^*(x^*); \quad w^* = 1, \quad \partial w^*/\partial y^* = 0. \tag{B.6}$$

The integral form of the energy equation is:

$$\frac{d}{dx^*} \int_0^{-t^*} T^*\, dy^* + T^*_{-t^*} \frac{dt^*}{dx^*} = \left.\frac{\partial T^*}{\partial y^*}\right|_{-t^*} - \left.\frac{\partial T^*}{\partial y^*}\right|_i. \tag{B.7}$$

For $t^* < 1$ (thermal boundary-layer region) we assume:

$$T^* = T_i^*(x^*)\left[1 + 2\left(\frac{y^*}{t^*}\right) + \left(\frac{y^*}{t^*}\right)^2\right]. \tag{B.8}$$

This second-order polynomial satisfies the following boundary conditions:

$$\text{at} \quad y^* = 0: \quad T^* = T_i^*(x^*) \tag{B.9}$$

$$\text{at} \quad y^* = -t^*: \quad T^* = 0, \quad \frac{\partial T^*}{\partial y^*} = 0. \tag{B.10}$$

Once $t^* = 1$ we obtain

$$T^* = T_i^* + F^*(x^*)(y^* + 0{\cdot}5\, y^{*2}) \tag{B.11}$$

which satisfies the following boundary conditions:

$$\text{at} \quad y^* = 0: \quad \frac{\partial T^*}{\partial y^*} = F^*(x^*), \quad T^* = T_i^*(x^*) \tag{B.12}$$

$$\text{at } y^* = -1: \quad \frac{\partial T^*}{\partial y^*} = 0. \tag{B.13}$$

Substitution of the polynomials into the integral equations, and using the matching conditions, equations (11–12) yield the following set of six equations for the unknowns $F^*$, $v_i^*$, $\delta^*$, $\xi$, $T_i^*$ and $w_i^*$:

$$F^* = \frac{2}{3}\frac{\mathrm{d}}{\mathrm{d}x^*}\left(\frac{T_i^{*2}}{F^*}\right); \quad t^* < 1 \tag{B.14.1}$$

$$F^* = \frac{\mathrm{d}}{\mathrm{d}x^*}(T_i^* - \tfrac{1}{3}F^*); \quad t^* = 1 \tag{B.14.2}$$

$$v_i^* = -\frac{F^*}{\lambda^*} \tag{B.15}$$

$$\frac{\mathrm{d}\delta^*}{\mathrm{d}x^*} - \frac{10P^*}{\partial^*} = 5v_i^* \tag{B.16}$$

$$\frac{\mathrm{d}}{\mathrm{d}x^*}\left[(w_i^* - 1)\,\delta^*\xi\left(-\tfrac{1}{3} + \tfrac{1}{6}\xi - \tfrac{1}{30}\xi^2\right)\right] = v_i^*; \quad \xi < 1 \tag{B.17.1}$$

$$\frac{\mathrm{d}}{\mathrm{d}x^*}\left[(w_i^* - 1)\,\delta^*\left(-\frac{1}{3} + \frac{1}{6\xi} - \frac{1}{30\xi^2}\right)\right] = v_i^*; \quad \xi > 1 \tag{B.17.2}$$

$$w_i^* = \frac{1}{1 + 0{\cdot}5\,\xi\delta^* v_i^*\,Se/P^*}. \tag{B.18}$$

Since $w_i^*$ and $T_i^*$ are related, another equation is required. It is derived from equation (12), where the appropriate relationship between temperature and vapor pressure is used (see Appendix C).

For the region where $x^* < \frac{1}{12}$ ($t^* < 1$) a closed form solution of the set is found and the results are:

$$T_i^* = \text{constant (hence } w_i^* \text{ equals constant)} \tag{B.19}$$

$$F^* = T_i^*/\sqrt{(3x^*)} \tag{B.20}$$

$$v_i^* = -T_i^*/[\lambda^*\sqrt{(3x^*)}] \tag{B.21}$$

$$\delta^* = B\sqrt{(P^*x^*)} \tag{B.22}$$

$$\xi = \frac{6N}{(\sqrt{3})\,B(w_i^* - 1)}; \quad \xi < 1 \tag{B.23.1}$$

$$\xi = \frac{1}{2 - \dfrac{12}{\sqrt{3}}\dfrac{N}{B(w_i^* - 1)}}; \quad \xi > 1 \tag{B.23.2}$$

and the values for $w_i^*$ are reported in equations (23) and (24). Note that all the variables are given in terms of $T_i^*$ or $w_i^*$ which were found to be constant. The solution for $T_i^*$ and $w_i^*$ (and thereby for all the variables) is obtained when we combine the last equation (C.2) which relates $w_i^*$ to $T_i^*$ through the vapor pressure–temperature correlation with equations (23) and (24) and solve both equations simultaneously. This procedure, which was used also for the exact solution, can be performed most conveniently graphically as illustrated in Fig. 2.

For the region where $x^* > \frac{1}{12}$ ($t^* = 1$) the above mentioned set of equations were simultaneously numerically integrated. For this purpose the equations are first brought into a form where the Runge–Kutta method for numerical integration can be applied. The initial values at the starting point $x^* = \frac{1}{12}$ are taken from the analysis for $x^* < \frac{1}{12}$.

It should be mentioned that in all calculations, only the first order terms for $\xi$ in equation (B.17) were retained. Retention of higher order terms proved to have an insignificant effect on the results, while considerably complicating the algebra.

## APPENDIX C

### *The Relationship Between $w_i^*$ and $T_i^*$*

For water: the vapor pressure–temperature correlation [11] is:

$$\ln_{10}\frac{P}{E} = A - B\ln_{10}T + CT - D/T \tag{C.1}$$

where $A = 28{\cdot}59051$, $B = 8{\cdot}2$, $C = 2{\cdot}4804 \times 10^{-3}$, $D = 3142{\cdot}31$, $E = 750{\cdot}062$, $P =$ Vapor

pressure in mm Hg, $T$ = Temperature in degrees Kelvin.

Substitution of the last equation into equation (7) yields the following relationship:

$$\log_{10}\frac{1-w_\infty w_i^*}{1-w_\infty\left(1-\frac{M_v}{M_g}\right)w_i^*}+B\ln_{10}\frac{T_i}{T_\infty}$$

$$-C(T_i-T_\infty)+D\left(\frac{1}{T_i}-\frac{1}{T_\infty}\right)=0 \qquad \text{(C.2)}$$

where $M_v = 18{\cdot}02$ and $M_g = 28{\cdot}97$.

For carbon tetrachloride: the vapor pressure–temperature relationship was correlated [7, 8] and found to be:

$$\ln_{10}P = -\frac{1719{\cdot}16}{T}+7{\cdot}8021. \qquad \text{(C.3)}$$

The relationship between $w_i^*$ and $T_i^*$ has the form of equation (C.2) where:

$$B = C = 0, \qquad D = 1719{\cdot}16, \qquad M_v = 153{\cdot}84.$$

$P$ and $T$ are the same units as before.

For convenience in practical applications there relations are plotted in Figs. 9 and 10.

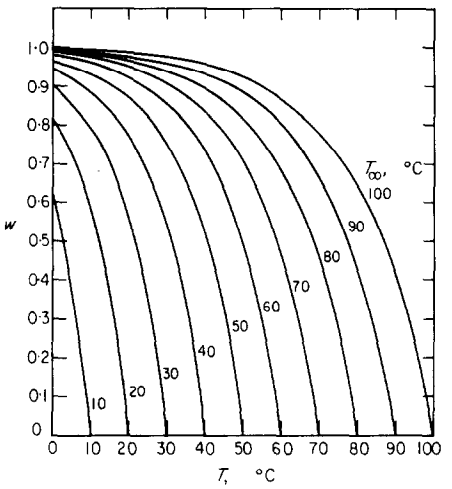


FIG. 9. $w$ vs. $T$ for various bulk saturation temperature of water.

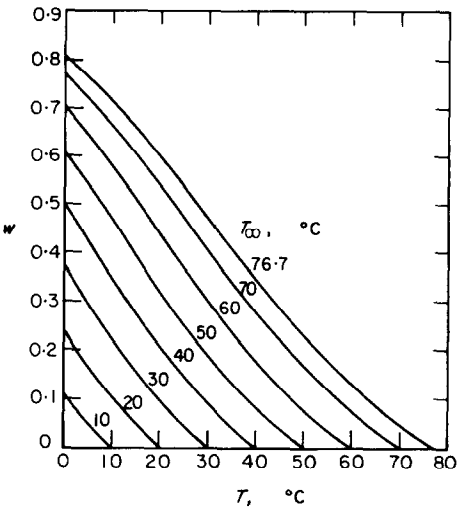


FIG. 10. $w$ vs. $T$ for various bulk saturation temperatures of carbon tetrachloride.

**Résumé**—Ce travail analyse l'effet des impuretés d'un gaz non condensable présent dans le sein d'une vapeur au cours de la condensation en contact direct. Le modèle physique est un écoulement laminaire libre qui est exposé à une atmosphère de sa propre vapeur contenant le gaz inerte. La solution est basée sur les équations de conservation de la couche limite utilisant une solution de similitude exacte et une méthode intégrale approchée.

La théorie prédit une diminution des densités de flux de chaleur près du "bord d'attaque" (petits $x^*$), qui peut être importante selon la concentration du gaz noncondensable et la force motrice thermique. Cet effet est accentué aux pressions les plus faibles. Loin en aval ($x^* > 1$) l'effet inverse est observé, c'est-à-dire que le flux de chaleur local devient beaucoup plus élevé comparé au cas sans la présence de gaz noncondensables.

**Zusammenfassung**—Der Einfluss von Verunreinigungen eines Dampfes durch Inertgase auf die Kondensation wird untersucht. Als physikalisches Modell liegt eine freie laminare Strömung, die ihrem eigenen durch Inertgase verunreinigten Dampf ausgesetzt ist, zugrunde. Die theoretische Lösung basiert auf

den Erhaltungssätzen für die Grenzschicht, wobei ein exaktes Ähnlichkeitsgesetz und eine angenäherte Integralmethode verwendet wird.

Die Analyse sagt eine Erniedrigung der lokalen Wärmeübergangszahl in der Nähe der "Anströmkante" ((kleines $x^*$) voraus, die je nach Inertgaskonzentration und treibender Temperaturdifferenz bedeutend sein kann. Dieser Einfluss ist grösser bei niedrigeren Drücken. Weit stromabwärts ($x^* > 1$) hingegen ist die örtliche Wärmestromdichte viel grösser als bei Abwesenheit der Inertgase.

**Аннотация**—В данной работе анализируется влияние примесей неконденсируемого газа к пару при прямой контакной конденсации. Физическая модель представляет собой свободный ламинарный поток в атмосфере пара, содержащего инертный газ. Решение основывается на уравнениях сохранения пограничного слоя с использованием точного автомодельного решения и приближенного интегрального метода. Дается расчёт снижения скорости теплообмена для малых $x^*$. Оно может быть значительно в зависимости от концентрации неконденсируемого газа и термической движущей силы. Этот эффект отчетливее проявляется при низких давлениях. Далеко вниз по течению ($x^* > 1$) наблюдается противоположное влияние, а именно, локальный тепловой поток становится намного больше по сравнению со случаем отсутствия неконденсируемых газов.